Biophysical Journal, Volume *110*

Supplemental Information

Dissociation of a Dynamic Protein Complex Studied by All-Atom Molecular Simulations

Liqun Zhang, Susmita Borthakur, and Matthias Buck

Supplementary Information

Dissociation of a Dynamic Protein Complex studied by All Atom Molecular Simulation

L. Zhang, S. Borthakur, and M. Buck

SUPPLEMENTARY EXPERIMENTAL METHODS, ANALYSIS, AND DISCUSSION

Binding affinity and kinetics of mutants by SPR measurement and comparison with MD simulations

Surface Plasmon Resonance (SPR) was carried out as follows: The proteins were dialyzed against a buffer consisting of 10 mM HEPES at pH 7.4, 150 mM NaCl, 1 mM TCEP-HCl and 0.005% surfactant P-20. SPR was measured on a Biacore T100 biosensor instrument (GE Healthcare) at 25°C. Proteins were immobilized on CM5 sensor chips using amine coupling (EphA2 SAM wild type: 150 RU {refractive units}, K956D: 180 RU, and R957D: 160 RU). Control surfaces were prepared with bovine serum albumin. Interaction experiments were carried out by injecting a series of concentrations of wild type or mutant SHIP2 SAM at a flow rate of 65 µl min^{-1}. The dissociation of the proteins was monitored over 1200 sec and then the surfaces were regenerated by two sequential 30 sec injections of 25 mM NaOH to dissociate bound SHIP2. The control response (a possible non-specific interaction with chip-bound Bovine serum albumin) as well as the baseline were subtracted [25]. The data were then fitted to a 1:1 binding model (for the wild type and K956D) and Heterogeneous ligand model (for R957D) using BIAevaluation 2.0 Software (GE healthcare, USA) and Origin 8.1 (OriginLab, Northampton, MA). The dissociation constants (K_D) were also independently determined from the fitting of the equilibrium binding data to 1:1 Langmuir model.

Kinetic rate measurements over a range of concentrations partially support the equilibrium binding data. The mutants have slower association rates (k_a), most pronounced in the case of the swap-mutant2 (R957D/D1223R) complex (Figure S3 c & d and Table S1). A slower association rate is expected because the electrostatic surface (displaying a large amount of charge degeneracy) is disrupted by the mutation (Fig. S5). Surprisingly, the dissociation rate (k_d) is not substantially changed for the K956D/D1235K complex. In the case of the R957D/D1223R complex, the dissociation data does not fit the 1:1 binding model well and were also fitted to the heterogeneous ligand model (Fig S4). Here, an increased rate of dissociation (by ~8-fold relative to wild type) was seen in the fast phase. Overall, the decreased affinity and slower association rates determined by the SPR analyses are consistent with the lower stability of the mutant SAM:SAM complexes observed in the simulations.

The experimental SPR data confirm slower association kinetics for the mutants compared to the wild type. (Table S1). The decrease in association rates is in accord with a diminished net electrostatic surface for steering the encounter complexes. However, in terms of the dissociation kinetics it is difficult to compare the timescale of the simulation to macroscopic measurements. While we have no evidence of interference by transport effects [55], the dissociation kinetics are at the upper limit of detection by SPR [56] and may still reflect a surface phenomenon. Remarkably, to our knowledge no direct comparison between SPR derived dissociation kinetics and simulations/even coarse-grained or Brownian dynamics has been published. (Our studies to define kinetics by NMR relaxation dispersion measurements or stop flow fluorescence measurements are on-going but suggest events occur on the low ms-time scale). In accord with a recent study [57,58 which also suggest a 10^3 fold discrepancy, in this case between computed energies/dissociation kinetics and Kd], it is likely that the dissociation process seen in the simulations is accelerated; the barriers to interconversion and protein separation may be low and the solvent dynamics of the TIP3P water model used [28], is 2.5-fold too fast [57]. As a note, a number of reports have recently questioned whether the current forcefields are accurate enough for simulating protein-protein association processes and suggest that the protein interactions may be stronger than in reality [59,60]. However, the fast dissociation kinetics and lack of recapture observed here would suggest the opposite.

Details of the protein dynamics analysis and discussion of its relative contribution compared to other thermodynamic changes upon protein dissociation

The contacting surface area was calculated as the difference of the solvent accessible surface between the free proteins and complex using the Lee and Richards algorithm in CHARMM (probe radius of 1.4 Å). Contributions to the solvent accessible surface from polar- and non-polar groups were considered separately. For this, atoms are classified into two types: nonpolar atoms (C, HP, HA, HB, HA1, HA2, and HA3) and polar atoms (O, N, S, P, H, HC, HR1, HR2, HR3, and HS – using CHARMM nomenclature for atom types). The hydrogen bond analysis used the standard distance cut-off of 3.5 Å and an angle cut-off of 90 degrees from linearity between donor-hydrogen and acceptor. The van der Waals and electrostatic interaction energies between proteins were calculated using the CHARMM program with the standard C36 forcefield and cut-offs. The solvation free energy was calculated with PBEQ [30] using a dielectric constant for the reference environment and protein interior of 1, while the solvent dielectric constant was set to 80. Although the change in solvation energy calculated this way appears to be an order of magnitude larger than estimated by other criteria, such as change in solvent accessible surface area (see below) the magnitude was consistent with other free energy calculations [30]. Recently, more advanced free energy perturbation methods are being developed [e.g. 61,62] but they are computationally expensive and beyond the scope of this report. However, we believe that the general trend and timing of the change is meaningful.

The protein entropy was estimated using a quasi-harmonic (Q.entropy) approach [31] as implemented in Wordom [32] for four representative 100 ns segments of a 2.4 μs wild type trajectory [24] (started from a cluster2 structure) and four 100 ns segments of a trajectory after SAM-SAM domain center of mass separation is greater than 40Å (Fig. S8, later part not shown). {The finding that no common dissociation pathways are observed, as well as the limitations in sampling, limited our analysis to that of the starting and end-points. Analysis on other separation trajectories gives similar results}. Protein residues were classified into those located at the predominant interacting surface, occasional and non-interacting surfaces (refer to Table S3 for residue listing). The free energy change due to altered protein dynamics (i.e. entropy change multiplied by the temperature, 300K) is scaled by the total number of atoms for each grouping of residues. These data and also the extent of the changes are given in Table S4. An alternative method estimates entropy differences following the approach of Yang and Kay [33] due to changes in bond motions of main- and sidechain N-H, C-H and C=O groups using Lipari-Szabo order parameters, S^2. Correlation times and S^2 were calculated using the NMR module in CHARMM. A cut-off for the correlation function of 3.3 ns was used, which is the estimated average correlation time for global motions of the free proteins and of the protein complex scaled by the discrepancy between TIP3P and real water motion [see ref. 57]. A cut-off value of 1.1 ns was used for each correlation function derived internal correlation times to determine whether the individual correlation function is well converged. A number of bond vectors were eliminated from the calculation because their motions had not converged by this criterion; thus between 3.7% (of mainchain N-H groups) to 15.7% (of sidechain C=O groups) of the X-H and C=O bonds were excluded. Similarly to the Q.entropy, the uncertainty was estimated from four 100 ns windows of a simulation of the wild type protein-protein complex (Table S5). The total free energy contribution due to a protein entropy change of 63.4 kcal mol^{-1} of 2180 atoms of the Q.analysis compares with 31.7 kcal mol^{-1} for 887 bonds from the S^2 entropy analysis, suggesting the latter analysis captures around 50% of the dynamic changes. The difference is consistent with the lesser number and type of atoms, as well as with the motions monitored.

Several methods have been used to estimate the contribution to entropy changes from the difference in protein dynamics between different states (usually bound – free) of proteins. Overall these estimates are similar in magnitude [e.g. 63-66, 49] and we have only used one method to estimate entropy from order parameters here. A second issue concerns the relative contribution of the protein entropy changes compared to other thermodynamic contributions. Following Wand and colleagues, as well as others, the total binding entropy (equivalent to the ITC derived value of $\Delta S*T$ = 4.7 kcal/mol), $T*\Delta S_{bind}$, is given by $T*\Delta S_{bind} = T* (\Delta S_{conf} + \Delta S_{sol} + \Delta S_{RT} + \Delta S_{other})$ [e.g. 47]. Here, ΔS_{sol} can be estimated using the change in non-polar and polar accessible surface area (ΔASA = buried surface area, denoted BSA above) as $\Delta S_{sol} = \ln (T/385) * (0.45\ \Delta ASA_{nonpolar} - 0.26\ \Delta ASA_{polar})$ [67]. The solvent accessible surface buried in the wild type complex is approx. 800 $Å^2$ with 60% non-polar vs. 40% polar, yielding a value of approx. -9.5 kcal/mol for $T*\Delta S_{sol}$. The entropy change due to change of rotational and translational entropy is 5R (where R is the gas constant) or 3.0 kcal/mol for $T*\Delta S_{RT}$ [68]. If we presume ΔS_{other} to be negligible, this would yield a value of 11.2 kcal/mol for

$T^*\Delta S_{conf.}$. This is the parameter we tried to capture by the two protein entropy analyses above. However, the total $T^*\Delta S$ values are 63.4 kcal/mol for the quasi-harmonic analysis and 31.7 kcal/mol for the order parameter analysis. We noted that the order parameter analysis yields an estimate for entropy change that is 50% below that from the quasi-harmonic analysis. This is in part because, as noted above, fewer atoms were considered, but also because the S^2 analysis does not consider motions slower than the correlation time cut-off or vibrational entropy with motions that do not involve bond rotation. Then, there remains a discrepancy between the estimated values for $\Delta S_{conf.}$ using the calculation above and the values calculated from the quasi-harmonic/order parameter analysis, suggesting that the difference of -20.5 kcal/mol would need to be absorbed by the ΔS_{other} term (in the case of the S^2 derived $T^*\Delta S_{conf.}$). This magnitude of discrepancy is not unusual (e.g. a value of 18.5 kcal/mol has been estimated in a study of Calmodulin variants binding to peptides [69], a protein that is similar in terms of the interacting surface area to the SAM domains). It should be noted that unlike reported in a few recent analyses [70,71], the entropy analyses described above do not consider correlated motions. However, the difference in ΔS_{conf} due to locally correlated bond motions is small (< 20%) compared to the changes considered above.

SUPPLEMENTARY REFERENCES:

55. Myszka, D. G. 1997. Kinetic analysis of macromolecular interactions using surface plasmon resonance biosensors. *Curr. Opin. Biotech.* 8:50-7.
56. Schmuck, P., and H. Zhao. 2010. The role of mass transport limitation and surface heterogeneity in the biophysical characterization of macromolecular binding processes by SPR biosensing. *Methods in Mol. Biol.* 627:15-54.
57. Mahoney, M.W., and W. L. Jorgensen. 2001. Diffusion constant of the TIP5P model of liquid water. *J. Chem. Phys.* 114:363-6.
58. Milev, S., S. Bjelić, ..., I. Jelesarov. 2007. Energetics of peptide recognition by the second PDZ domain of human protein tyrosine phosphatase 1E. *Biochemistry.* 46:1064-78.
59. Abriata, L. A., and M. D. Parado. 2015. Assessing the potential of atomistic molecular dynamics simulations to probe reversible protein-protein recognition and binding. *Sci. Reports.* 5: 10549.
60. Petrov, D., and B. Zagrovic. 2014. Are Current Atomistic Force Fields Accurate Enough to Study Proteins in Crowded Environments? *PLoS Comp. Biol.* 10:e1003638.
61. Ulucan, O., T. Jaitly, and V. Helms. 2014. Energetics of Hydrophilic Protein–Protein Association and the Role of Water. *J. Chem.Theory. Comp.* 10:3512-24.
62. Gumbart, J. C., B. Roux, and C. Chipot. 2013. Efficient Determination of Protein–Protein Standard Binding Free Energies from First Principles. *J. Chem. Theory Comput.* 9:3789-98.
63. Kasinath, V., K. A. Sharp, and A. J. Wand. 2013. Microscopic insights into the NMR relaxation-based protein conformational entropy meter. *J. Am. Chem. Soc.* 135:15092-100.
64. Tzeng, S. R., and C. G. Kalodimos. 2012. Protein activity regulation by conformational entropy. *Nature.* 488:236-40.
65. Trbovic, N., J. H. Cho, ..., A. G. 3rd Palmer. 2009. Protein side-chain dynamics and residual conformational entropy. *J. Am. Chem. Soc.* 131:615-22.
66. Glass, D. C., M. Krishnan, ..., J. Baudry. 2013. Three entropic classes of side chain in a globular protein. *J. Phys. Chem. B.* 117:3127-34.
67. Hilser, V. J., E. B. García-Moreno, ..., S. T. Whitten. 2006. A statistical thermodynamic model of the protein ensemble. *Chem. Rev.* 106:1545-58.
68. Yu, Y. B., P. L. Privalov, and R. S. Hodges. 2001. Contribution of translational and rotational motions to molecular association in aqueous solution. *Biophys. J.* 81:1632-42.
69. Marlow, M. S., J. Dogan, ..., A. J. Wand. 2010. The role of conformational entropy in molecular recognition by calmodulin. *Nat. Chem. Biol.* 6:352-8.
70. Li, D-W, and R. Bruschweiler. 2012. Dynamic and Thermodynamic Signatures of Native and Non-Native Protein States with Application to the Improvement of Protein Structures. *J.Chem.Theory. Comp.* 8:2531-2539.
71. Sharp, K. A., E. O'Brien, ..., A. J. Wand. 2015. On the relationship between NMR-derived amide order parameters and protein backbone entropy changes. *Proteins.* 83(5): 922-30.

SUPPLEMENTARY TABLES:

Table S1. Comparison of the equilibrium binding and kinetic parameters of the wt and mutant SAM:SAM complexes.

Complex EphA2/SHIP2	**K_D (μM)**	**k_a (x10^3 M s^{-1})**	**k_d (x10^{-3} s^{-1})**	**k_{a2} (x10^3 Ms^{-1})**	**k_{d2} (x10^{-3} s^{-1})**
wild type/wild type	2.2 ± 0.2	16.4 ± 0.2	35 ± 2	-	-
K956D/D1235K	20.3 ±0.3	4.38 ± 0.1	89 ± 17	-	-
R957D/D1223R	106 ± 8.2	3.45 ± 0.02	285 ± 10	0.11 ±0.002	7 ± 0.8

Table S2. Analysis of structures before and during protein dissociation for trajectories corresponding to Figs. 3 and 4: Parameters for the three starting points (clusters1-3) of the R956D/D1223R mutant complex (after 20ns of NAMD simulation) and for distinct points of the zoomed in separation trajectories including RMSD, crossing angle between helices5 of the EphA2 SAM and SHIP2 SAM domains calculated using the method published previously [24], center of mass distance (COM), buried surface area (BSA) buried (total, polar/non-polar and ratio), hydrogen-bonds (Hbs): protein-protein, protein-solvent, the number of waters within 3.5 Å of protein, solvation free energy calculated with PBEQ [30] and waters bridging between the EphA2 and SHIP2 interfaces (less than 3.5 Å distant from both). Each parameter was calculated and averaged over 1 ns with 0.5 ns on each side of the stated time-point. For comparison data for 5ns into the wild type trajectories, started with each of the clusters1-3, are shown [24].

(a) for trajectory corresponding to Fig. 3,4 started with cluster2.

Time	WT	MutNAMD	1ns	5ns	7.5ns	10ns	12.5ns	18ns	20ns	22.5ns	26ns
COM (Å)	23.4±0.3	25.4±0.6	27.9±0.3	26.9±0.5	29.2±0.3	30.1±0.4	29.1±0.5	30.0 ±0.6	33.0±1.0	30.5±0.5	53.2±0.9
RMSD (Å)	3.4±0.4	5.7±0.4	5.3±0.2	5.1±0.1	7.4±0.3	8.8±0.2	9.5 ±0.3	11.1 ±0.1	13.1±0.2	10.4±0.1	19.7±0.3
Angle (°)	55.3±6.6	55.7±5.2	52.9±5.0	62.0±6.5	47.7±5.7	87.9±5.0	103 ±4.8	95.2±2.1	130.1±4	105.1±6	90.4±3
BSA (Å²)	898±76.2	714±61.3	634±29	501±30	596±42	406±26	444±23	387±53.6	82.2±74	236±57.4	~ 0
BSA-np (%)	59.3±4.0	63.6±5.6	64.2±2	62.7±4	61.7±5	50.3±5	53.9±5	61.8±9	31.9±25	57.1±11	N/A
BSA-p (%)	40.7±6.0	36.4±4.6	35.8±3	37.3±2	38.3±3	49.8±6	46.0±4	38.2±5	68.1±65	42.9±13	N/A
Number of waters	558±10.0	599±9.6	607±8.4	615±6	596±5.4	601±5.9	603±5.6	614.2±7.8	627.0±5.	612.±7.6	633±6.4
Hbs-protein-solvent	327±13.5	358±10	358±10.	353±8	347±11	345±9	337±7	353±8.6	356±9.4	353±6.3	360±11
Hbs-protein-protein	18.1±2.8	8.6±1.7	5.4±0.4	3.7±1.8	3.9±1.7	3.9±1.9	10.3±0.6	3.6±1.3	1.8±2.7	0.4±0.8	~ 0
ΔGs Solvation (kcal/mol) relative to Mut.NAMD	222 ±60	0 ±55	53±43	-56±31	139±56	29±29	133±35	-49±27	-217±53	-89±51	-333 ±49
Waters bridging interface	2.8±2.3	3.6±2.3	4.7±1.8	1.2±0.8	1.8±0.7	2.3±1.4	2.7±1.5	1.8±0.8	3.3±2.9	0.44±0.6	~ 0

Table S2 (b). Analysis of structures before and during dissociation for swap-mutant2 starting from cluster1 simulation results (corresponding to Fig. S6 and S7). See the description for Table S5a for details.

Time	WT	Mut.NAMD	1ns	5ns	7.5ns	10ns	12.5ns	18ns	20ns	22.5ns	26ns
COM (Å)	25.1±0.3	24.6±0.3	31.5±0.5	29.5±0.7	31.0±0.7	30.3±0.4	30.5±0.3	34.1±0.6	31.2±0.5	42.0±1.2	52.8±1.0
RMSD (Å)	2.3±0.3	5.8±0.2	12.4±0.1	11.7±0.1	11.4±0.2	11.3±0.1	11.6±0.1	11.0±0.3	10.6±0.2	15.4±0.3	18.9±0.5
Angle (°)	14.3±5.9	16.1±5.1	162.3±4.0	148.1±6.7	135.1±5.0	132.3±4.3	140.2±3.1	132.7±8.2	137.1±3.5	143.7±5.7	73.9±4.8
BSA (Å²)	692±45	767±56	286±45	303±41	236±17	254±17	292±25	174±29	233±17	~0	~0
BSA-np (%)	60.8±4.1	42.9±5.7	17.8±5.9	33.4±7	33.8±4	32.5±4	29.8±6	32.4±12.3	42.0±7	N/A	N/A
BSA-p (%)	39.2±4.5	57.1±3.4	82.2±11.6	66.7±8	66.2±7	67.5±8	70.2±4	67.6±6.2	58.0±4	N/A	N/A
Number of waters	585±12.9	596±8.6	614±6.7	619±9.1	612±5.3	609±8.5	612±1.6	634±2.7	617±9.5	627±5.6	645±7.1
Hbs-protein-solvent	344±15.4	350±10.0	333±8.9	345±9.4	341±6.3	340±9.3	342±8.5	350±5.0	345±7.7	358±2.9	361±5.9
Hbs-prot-protein	10.5±1.4	13.5±1.6	10.2±1.2	9.2±0.5	8.0±1.1	6.2±1.5	8.4±0.5	5.8±0.3	6.2±0.6	~0	~0
ΔGs Solvation (kcal/mol) relative to Mut.NAMD	-94 ±90	0 ±59	+151 ±40	151±53	116±57	166±45	190±42	160±33	-3±34	-113±53	-252 ±33
Bridging waters	3.3±2.1	4.9±1.5	12.1±1.5	0.9±0.4	5.6±1.5	6.4±2.0	6.1±2.00	0.9±0.5	5.2±2.1	~0	~0

Table S2 (c) Analysis of structures before and during protein dissociation for swap mutant2 simulation starting from cluster3 (corresponding to Fig. S8, S9). See legend for Table S5a for details.

Time	WT	Mut.NAMD	1ns	5ns	7.5ns	10ns	12.5ns
COM (Å)	25.5±0.3	26.9±0.3	27.5±0.3	28.3±0.3	30.9±0.4	34.1±0.8	44.3±1.8
RMSD (Å)	2.6±0.4	6.1±4.1	4.4±0.2	5.7±0.3	8.9±0.4	9.9±0.4	12.7±0.8
Angle (°)	100±10.5	105±6.4	103±3.0	98.7±5.9	67.7±4.00	81.1±5.9	53.9±10.8
BSA (Å²)	812±72.5	637±45.5	497±33.9	503±38.3	272±60.7	~0	~0
BSA-np (%)	50.2±4.3	57.1±3.4	65.4±5.3	77.9±5.7	42.8±9.7	N/A	N/A
BSA-p (%)	49.9±6.0	42.9±5.4	34.6±4.0	22.1±8.1	57.2±14.1	N/A	N/A
Number of waters	581±7.8	576±7.8	590±8.5	604±6.4	633±6.6	639±6.4	630±3.1
Hbs-protein-solvent	335±10.8	335±8.9	346±10.5	351±10.5	355±6.2	349±6.5	339±9.4
Hbs-protein-protein	16.0±3.2	12.5±1.2	8.4±0.6	0.8±1.5	6.4±2.3	~0	~0
ΔGs Solvation (kcal/mol) relative to Mut.NAMD	-130 ±70	0±43	-128±54	-155±58	-293±45	-199±63	-360±8
Bridging waters	3.5±2.7	8.7±2.9	2.5±1.4	3.9±3.0	~0	~0	~0

Table S3. Classification of protein residues according to the type of surface.

Class of residues	EphA2 SAM	SHIP2 SAM
at predominant interface	916, 917, 950-954, 956, 957, 960	1220-1223, 1226, 1227, 1230-1232, 1235, 1238
near interface/ sampled occasionally in mutants	918-921, 923, 924, 941, 942, 945, 946, 955	1224, 1229, 1233, 1234, 1237, 1241, 1242, 1246
not at interfaces (above) but on protein surface	909, 912, 913, 921, 925, 930, 936, 937, 939, 944, 949	1201, 1205, 1210, 1212, 1217, 1228, 1236, 1239, 1250, 1254

Table S4. The entropy increases at some but not all interaction interfaces upon protein dissociation, but it also decreases for a non-interface region of SHIP2. Entropy was calculated as described above in the method section. All values (except atom number and % differences) are in cal mol^{-1} $atom^{-1}$. Three classes of residues: predominant interface, low population interface, and non-interface are listed. Columns (bold headings): Values are given for entropies as Entropy*T, for the three different regions of the SAM-SAM complex; the % variation is an average over four 100 ns segments. The numbers of atoms involved in the analyses are shown within [ ] parentheses following the entropy values. The Temperature, T, was 300 K. In-between columns (headings in *Italics*): Shows the Entropy*T change, ΔEntropy*T, as an absolute difference value and in %, (given in [ ] parentheses) comparing the dissociated proteins with the complex. The total Entropy*T change upon dissociation, which is the sum of the values in columns multiplied in each case by the relevant number of atoms, is 63.4 $kcal.mol^{-1}$. Values with significant changes are given in bold.

	Predominant Interface Entropy*T [Number of atoms]	*av. Interface ΔEntropy*T [difference in %]*	**Low-pop Interface** Entropy*T [Number of atoms]	*av.low-pop Interface ΔEntropy*T [difference %]*	**Non-Interface** Entropy*T [Number of atoms]	*av. Non-Interface ΔEntropy*T [difference in %]*
EphA2						
mainchain	1297.8±0.7% [40]	**166.3 [+12.8%]**	1534.4±2.1% [68]	**85.3 [+5.6%]**	1469.9±1.5%[177]	41.6 [+2.8%]
sidechain	1197.4±1.5% [137]	**238.8 [+20.0%]**	1469.9±1.0% [238]	44.5 [+3.0%]	1333.7±1.4%[495]	10.8 [+0.8%]
SHIP2						
mainchain	1391.0±2.5% [44]	39.4 [+2.8%]	1355.2±1.5%[56]	10.0 [+0.7%]	1448.4±3.0% [161]	68.1 [+4.7%]
sidechain	1161.6±1.6% [132]	**80.3 [+6.9%]**	1434.0±0.8%[147]	48.8 [+3.4%]	1247.6±2.5% [485]	**-74.6 [-6.0%]**

Table S5. Dynamics changes (Entropy change*T) as evaluated by the analysis of Lipari-Szabo order parameters confirm that almost all interface sites in both domains have greater fluctuations in the free proteins compared to the complex. Some non-interface sites in SHIP2 SAM show moderately decreased dynamics upon dissociation. Dynamics changes by bond type are listed for the three classes of interface in cal mol^{-1} $bond^{-1}$, significant changes are given in bold. The total entropy*T change upon dissociation (= columns * relevant number of bonds) is 31.7 $kcal.mol^{-1}$. As would be expected from the nature of residues at the predominant interfaces (Arg/His/Lys on one side and Asp/Glu on the other), N-H/positively charged sidechain groups at the EphA2 interface experience the largest entropy increase, whereas for SHIP2 this is true for C=O/negatively charged groups. Changes away from these interfaces involve the opposite groups, consistent with the observation that those sidechains are the more prevalent at the infrequently interacting- and non-interacting surfaces.

Bond types	Predominant Interface ΔEntropy MC/SC [# bonds MC/SC]	Low-pop Interface ΔEntropy MC/SC [# bonds MC/SC]	Non-Interface ΔEntropy MC/SC [# bonds MC/SC]
EphA2			
N-H	**207.9**±14.3 / **71.7**±21.5 [9] / [12]	**121.5**±45.0 / 14.3±35.9 [14] / [24]	50.2±21.5 / 43.0±21.5 [28] / [11]
C-H	**243.8**±28.7/ **172.1**±50.2 [11] / [48]	78.9±50.2 / **93.2**±28.7 [14] / [62]	**86.0**±28.7 / 7.2±14.3 [30] / [104]
C=O	**229.4**±21.5 / N/A [7] / [0]	**114.7**±21.5 / -7.2±50.2 [16] / [10]	50.2±14.3 / **78.9**±21.5 [28] / [13]
SHIP2			
N-H	28.7±43.0 / 14.3±28.7 [11] / [3]	-14.3±43.0 / 14.3±28.7 [14] / [3]	-50.2±21.5 / **-71.7**±21.5 [28] / [23]
C-H	28.7±57.4 / **164.9**±78.9 [12] / [37]	-21.5±43.0/ 71.7±35.9 [14] / [60]	**-107.6**±28.7 / 43.0±21.5 [34] / [122]
C=O	14.3±35.9 / **93.2**±35.9 [10] / [7]	-35.9±21.5 / -21.5±21.5 [14] / [15]	**-71.7±28.7** / -28.7±21.5 [29] / [10]

SUPPLEMENTARY FIGURES:

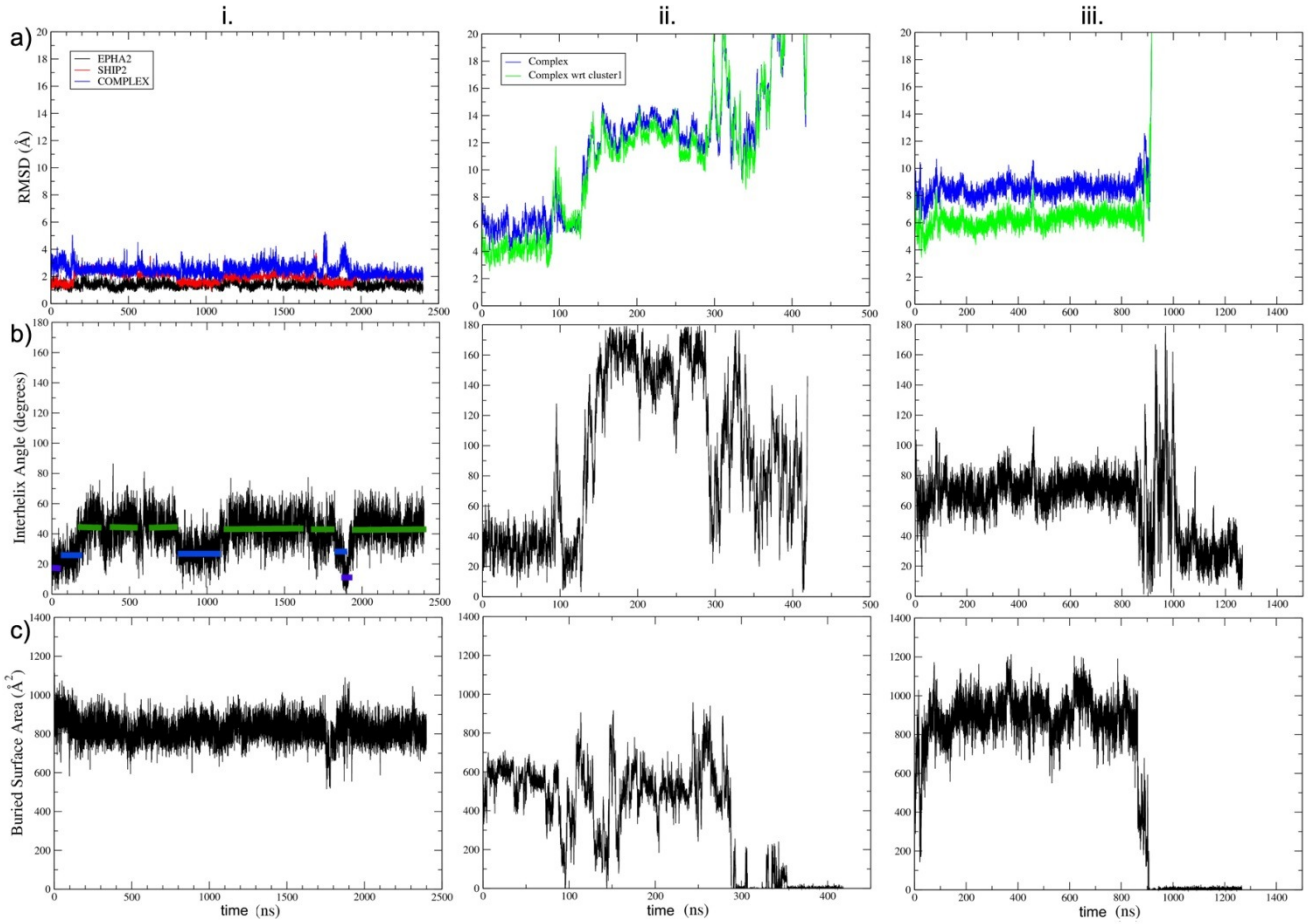

Figure S1 Fluctuations in the 2.4 μs trajectories starting from different swap-mutant1 (K956D/D1235K) SAM-SAM complex configurations (clusters 1-3 as i., ii. and iii. respectively). (a) Mainchain RMSD (with respect to starting structure is shown in blue and with respect to the initial cluster1 configuration is shown in green). (b) Angle between helix5 of each domain shows the similarity to the original cluster geometry (green=cluster1; blue=cluster2). (c) Buried surface area.

Compared to wild type simulations reported before [24], the cluster1 configuration is sampled more frequently in panel a.i. Swap-mutant1 is most compatible with the cluster1 configuration: the relative population of cluster1 vs. 2 has shifted from 49% vs. 36% in the wild type [Fig. 2b in ref. 24] to 60% vs. 20% for this mutant.

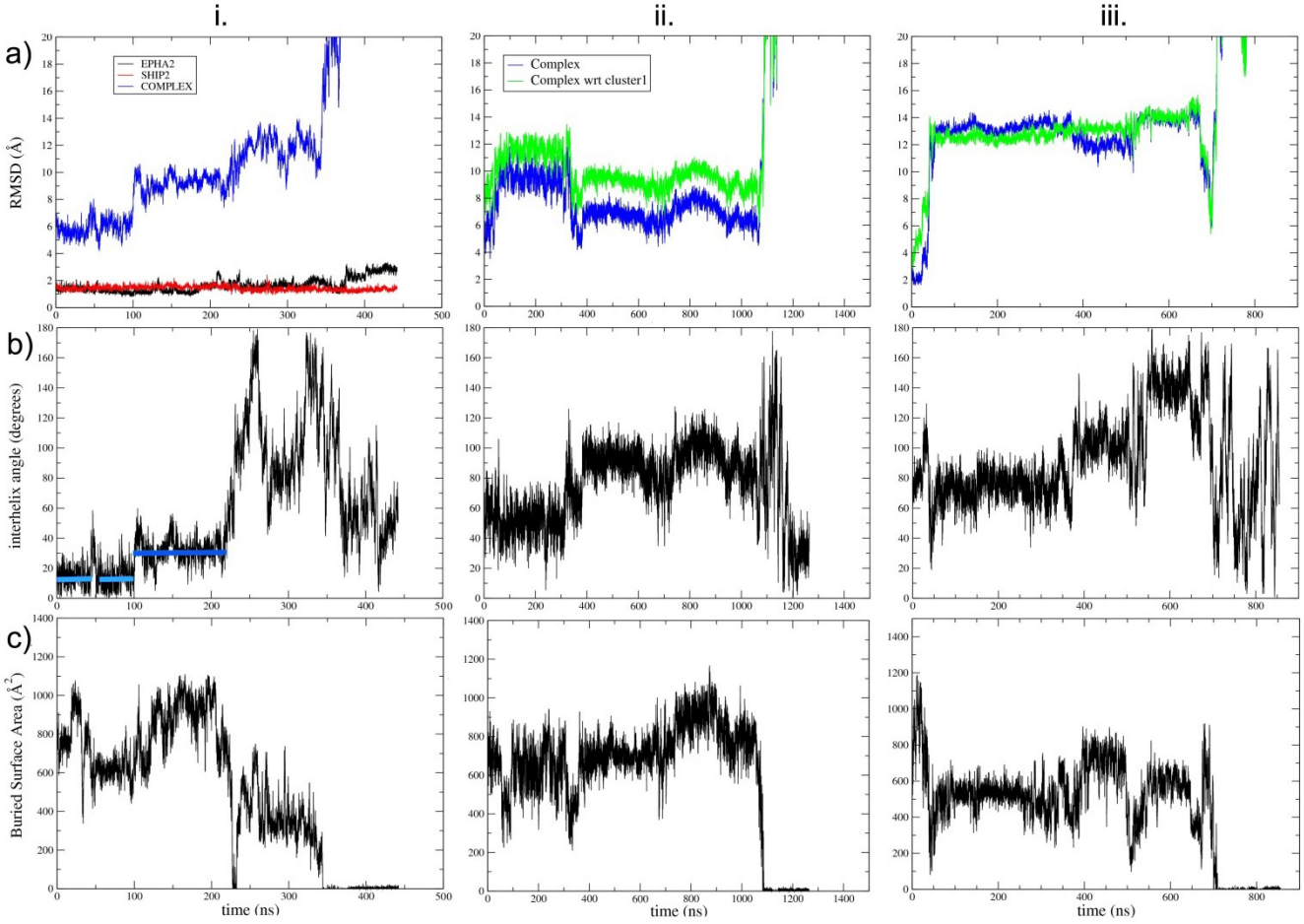

Figure S2 Fluctuations in the 2.4 μs trajectories starting from different swap-mutant2 (R957D/D1223R) SAM-SAM complex configurations (clusters 1-3 as i., ii. and iii. respectively). (a) Mainchain RMSD (with respect to starting structure, blue and cluster1 configuration, green). (b) Angle between helix5 of each domain, shows the similarity to the original cluster geometry (green=cluster1; blue=cluster2; however in this case the large RMSD shows structure is not populating cluster1). (c) Buried surface area.

In the case of the cluster1 started simulation (panel i), cluster2 is sampled more than in the wild type simulation (here 44% vs. 36% for cluster2 in Fig. 2b of ref. 24).

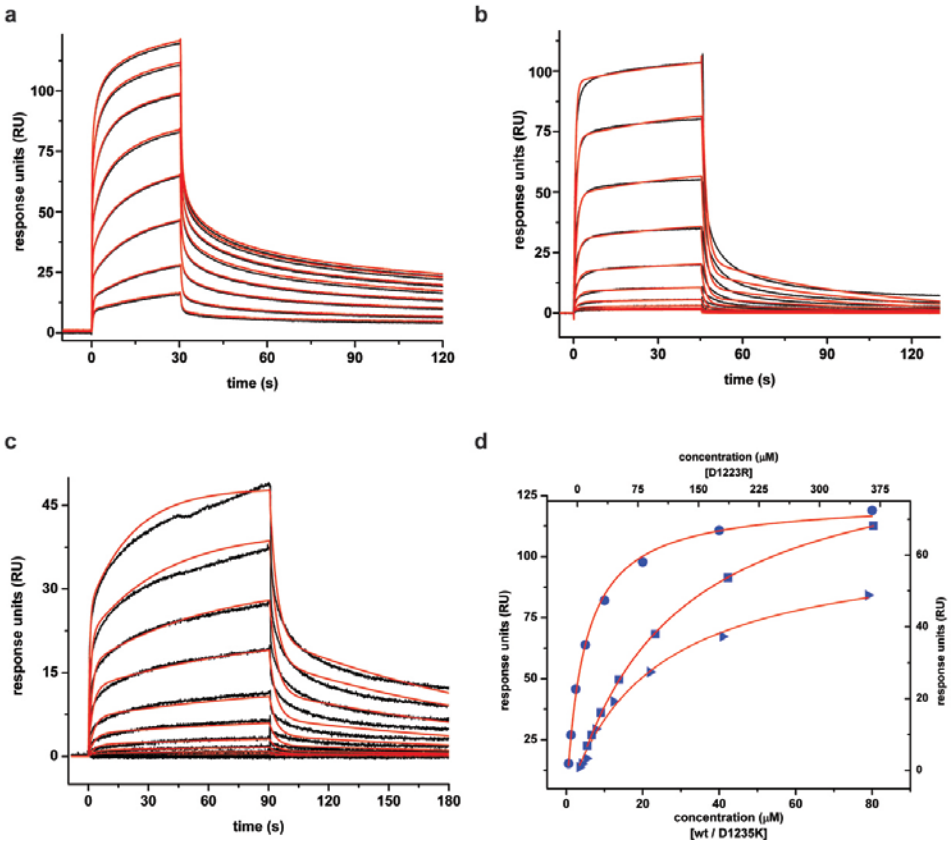

Figure S3. SPR analysis of binding of the wild type and the mutant complexes. The EphA2:SHIP2 SAM:SAM (a) and K956D/D1235K (b) data fit well to the 1:1 Binding model. (c) The kinetics of R957D/D1223R interaction fit the Heterogeneous Ligand model better. The experimental response curves for different concentrations are drawn in black and the corresponding fits are drawn in red. (d) The equilibrium binding data of the wild type (blue, filled circles, K956D/D1235K (blue, filled squares), and R957D/D1223R (blue, filled triangles) complexes were fitted to the 1:1 Langmuir model to estimate the dissociation constant (K_D). Note that due to the different concentration range for the R957D/D1223R, its x-axis is given above the plotted data and for the wild type protein and K956D/D1235K, below the data. The kinetic parameters are reported in Table S1.

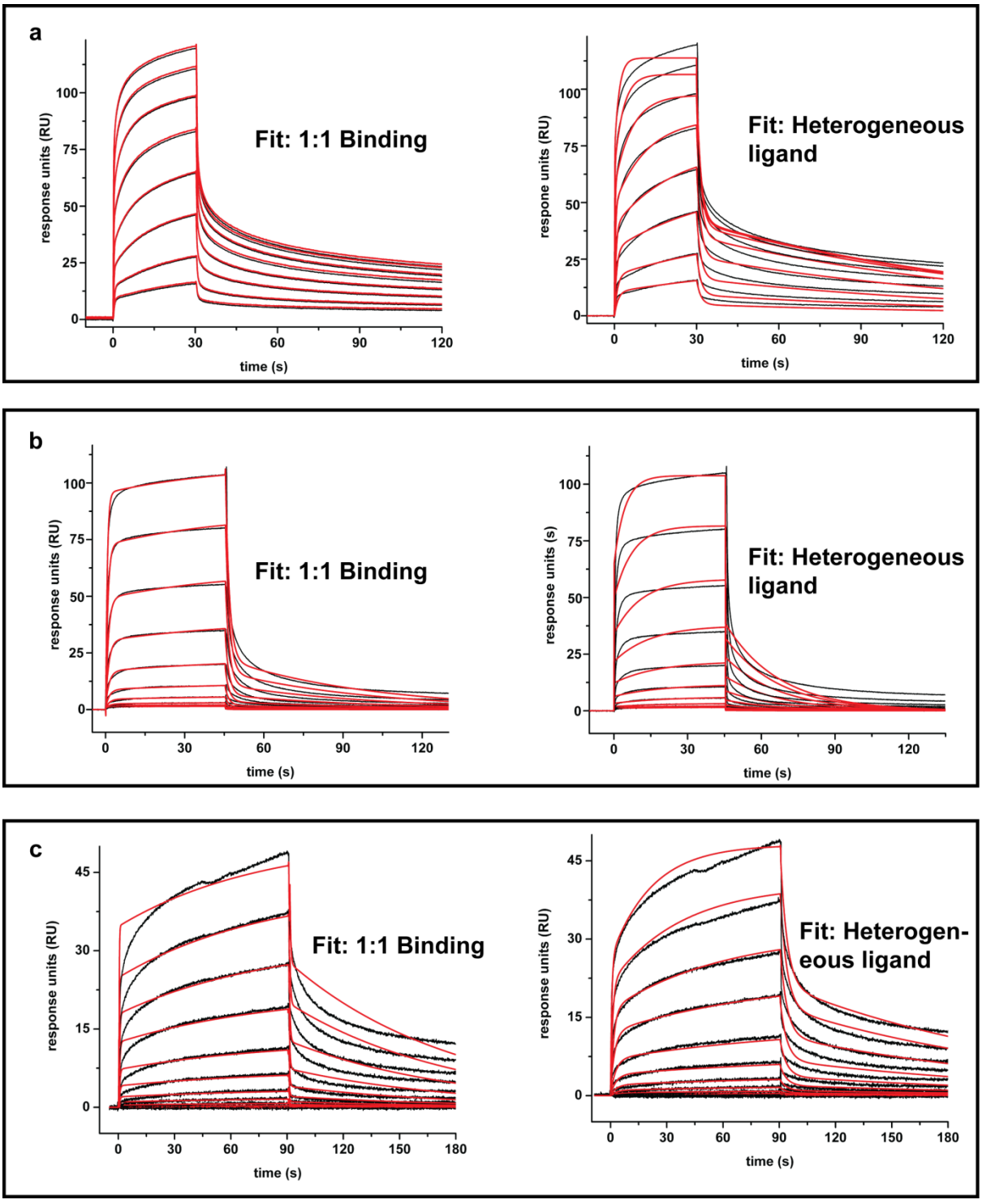

Figure S4. Comparison of the SPR kinetics data of the wt and mutant EphA2 SAM: SHIP2 SAM complexes fitted to the 1: 1 Binding and the Heterogeneous Ligand models. (a) The kinetics data of the wild type complex, (b) K956D/D1235K complex, and (c) R957D/D1223R complex. The R957D/D1223R data fits well to the Heterogeneous Ligand model, whereas, the wild type and the K956D/D1235K fit better to the 1:1 Binding model.

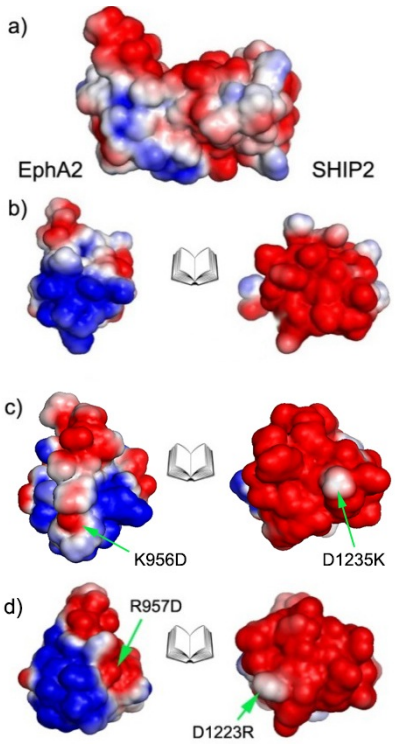

Figure S5. Swap mutations have a local effect on interface electrostatics. In the wild type SAM:SAM complex (a) 5 positive charges on the EphA2 interface meet 7 negatively charged residues on the SHIP2 side. (b) Complex shown as open book presentation, (c) and (d) with the mutations indicated by green arrows and residue labels. The electrostatic surface was calculated with the APBS module of pymol and is shown at ± 1 kT.

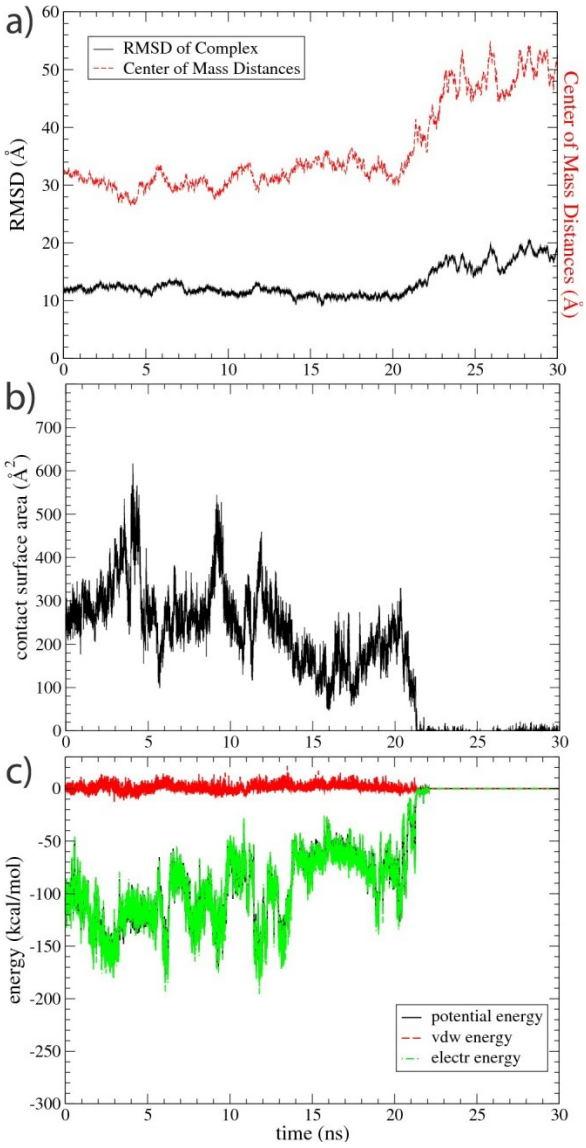

Figure S6. Analysis of a zoomed in region of the swap-mutant2 trajectory started with cluster1 configuration showing protein separation. (a) RMSD and center of mass separation. (b) Total solvent accessible surface area buried in complex. (c) Electrostatic and van der Waals potential interaction energy.

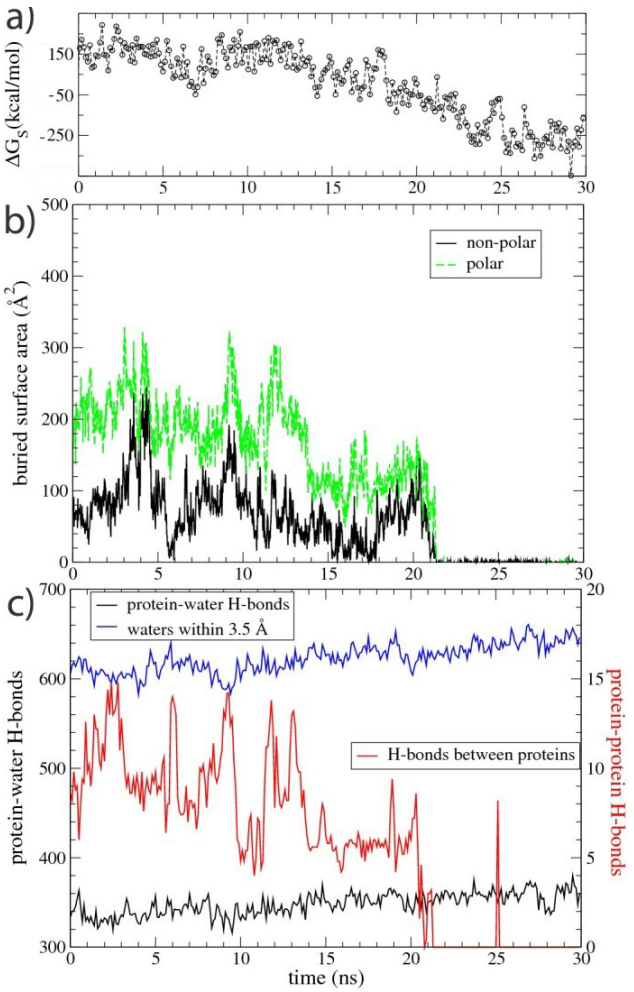

Figure S7. Analysis of a zoomed in region of the swap-mutant2 simulation, starting from cluster1. (a) Change in solvation free energy. (b) Polar and non-polar solvent accessible surface area buried at the protein interface. (c) Total number of protein-solvent hydrogen bonds (3.5 Å and 90 degree cutoff for distance, N-H O=C linearity) and number of water-protein contacts within 3.5 Å of the protein surface.

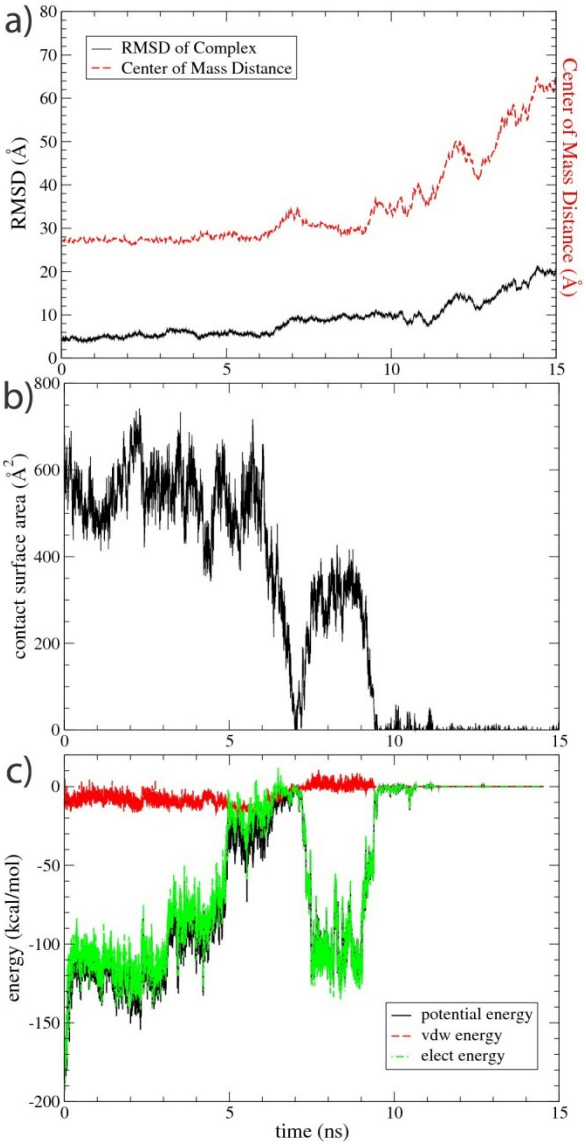

Figure S8. Analysis of a zoomed in region of the swap-mutant2 trajectory, started with cluster3 configuration, showing protein separation. (a) RMSD and center of mass separation. (b) Total solvent accessible surface area buried in complex. (c) Electrostatic and van der Waals potential interaction energy.

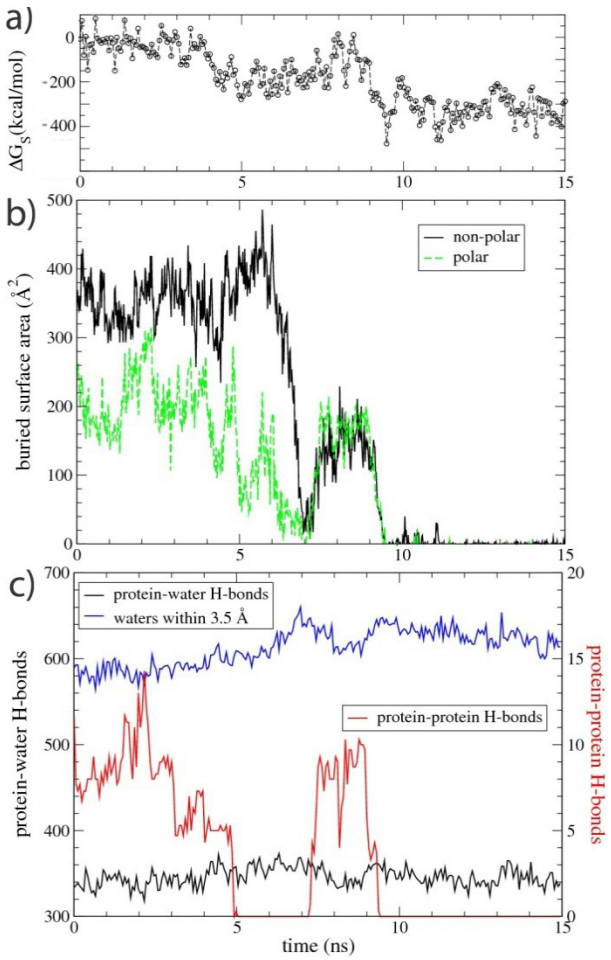

Figure S9. Analysis of a zoomed in region of the swap-mutant2 simulation started from cluster3. (a) Change in solvation free energy. (b) Polar and non-polar solvent accessible surface area buried at the protein interface. (c) Total number of protein-solvent hydrogen bonds (3.5 Å and 90 degree cutoff for distance, N-H O=C linearity) and number of water-protein contacts within 3.5 Å of the protein surface.

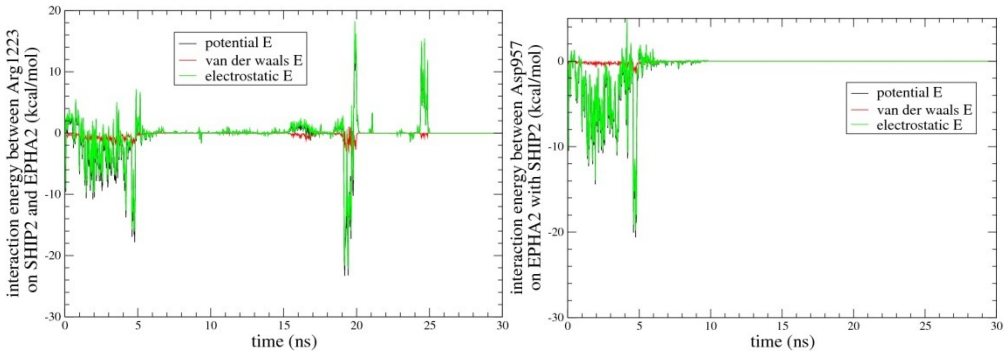

Figure S10. Interaction potential energy between mutated residues and their opposing interfaces (cluster2 started zoomed in swap.mutant2 trajectory). (a) SHIP2 Arg1223 with EphA2 and (b) EphA2 Asp957 with SHIP2, showing initially favorable interactions, followed by favorable interaction of Arg1223 and then repulsive interactions during the final separation process.

MOVIE:

Movie: The protein dissociation process of Fig. 2, 3 and Table of Content Figure, is shown with SAM domains in van der Waals space-filling representation. The trajectory is centered on the initial orientation of EphA2 SAM. Residues are colored as white: non-polar sidechains, green: hydrophilic and blue/red, positively and negatively charged sidechains, respectively. The mutated residues EphA2 R957D and SHIP2 D1223R are shown as 2x vdW radii spheres. The interaction exists at the start of the movie but is broken by the transitions. Eventually the mutated SHIP2 residue D1223R participates in a repulsive event with EphA2 Arginines (see Fig. S10).